

# Correlation of non-mass-like abnormal MR signal intensity with pathological findings surrounding pediatric osteosarcoma and Ewing's sarcoma

Karim Z. Masrouha · Khaled M. Musallam ·  
Alexis Bou Samra · Ayman Tawil · Rachid Haidar ·  
Zaher Chakhachiro · Said Saghie · Abeer Abdallah ·  
Raya Saab · Samar Muwakkit · Miguel R. Abboud ·  
Nabil J. Khoury

Received: 9 September 2011 / Revised: 27 October 2011 / Accepted: 19 February 2012 / Published online: 10 March 2012  
© ISS 2012

## Abstract

**Objective** The aim of this work was to determine the role of MRI in interpreting abnormal signals within bones and soft tissues adjacent to tumor bulk of osteosarcoma and Ewing's sarcoma in a pediatric population by correlating MR findings with histopathology.

**Materials and methods** Thirty patients met the inclusion criteria, which included (1) osteosarcoma or Ewing's sarcoma, (2) MR studies no more than 2 months prior to surgery, (3) presence of abnormal MR signal surrounding the tumor bulk, (4) pathological material from resected tumor. The patients received standard neoadjuvant chemotherapy. Using grid

K. Z. Masrouha · R. Haidar · S. Saghie  
Department of Surgery,  
American University of Beirut Medical Center,  
PO Box 11-0236, Riad El Solh,  
Beirut 1107 2020, Beirut, Lebanon  
e-mail: km34@aub.edu.lb

R. Haidar  
e-mail: rh00@aub.edu.lb

S. Saghie  
e-mail: ss15@aub.edu.lb

K. M. Musallam  
Internal Medicine Division of Hematology & Oncology,  
American University of Beirut Medical Center,  
PO Box 11-0236, Riad El Solh,  
Beirut 1107 2020, Beirut, Lebanon  
e-mail: kmm06@aub.edu.lb

A. B. Samra · A. Tawil · Z. Chakhachiro  
Pathology, American University of Beirut Medical Center,  
PO Box 11-0236, Riad El Solh,  
Beirut 1107 2020, Beirut, Lebanon  
e-mail: armasoub22@hotmail.com

A. Tawil  
e-mail: at04@aub.edu.lb

Z. Chakhachiro  
e-mail: z\_shak@hotmail.com

R. Saab · S. Muwakkit · M. R. Abboud  
Children's Cancer Center of Lebanon,  
American University of Beirut Medical Center,  
PO Box 11-0236, Riad El Solh,  
Beirut 1107 2020, Beirut, Lebanon  
e-mail: rs88@aub.edu.lb

S. Muwakkit  
e-mail: sm03@aub.edu.lb

M. R. Abboud  
e-mail: ma56@aub.edu.lb

A. Abdallah · N. J. Khoury (✉)  
Diagnostic Radiology,  
American University of Beirut Medical Center,  
PO Box 11-0236, Riad El Solh,  
Beirut 1107 2020, Beirut, Lebanon  
e-mail: nk01@aub.edu.lb

A. Abdallah  
e-mail: aa162@aub.edu.lb

maps on gross pathology specimens, the abnormal MR areas around the tumor were matched with the corresponding grid sections. Histopathology slides of these sections were then analyzed to determine the nature of the regions of interest. The MR/pathological correlation was evaluated using Mann–Whitney *U* test and Fisher's exact test.

**Results** Twenty-seven patients had osteosarcoma and three patients had Ewing's sarcoma. Of the studied areas, 17.4% were positive for tumor (viable or necrotic). There was no statistically significant correlation between areas positive for tumor and age, gender, signal extent and intensity on MRI, or tissue type. There was, however, a statistically significant correlation between presence of tumor and the appearance of abnormal soft tissue signals. A feathery appearance correlated with tumor-negative areas whereas a bulky appearance correlated with tumor-positive regions.

**Conclusions** MR imaging is helpful in identifying the nature of abnormal signal areas surrounding bone sarcomas that are more likely to be tumor-free, particularly when the signal in the soft tissues surrounding the tumor is feathery and edema-like in appearance.

**Keywords** Osteosarcoma · Ewing's sarcoma · MRI · Histology · Staging

## Introduction

Primary bone sarcomas are rare tumors, accounting for 1% of all malignancies and 6% of all new pediatric cancer cases diagnosed annually in the United States [1, 2]. Their prognosis has significantly improved over the past three decades, largely due to precision of staging by imaging, chemotherapeutic protocols, and advancements in surgical techniques [3]. These advancements have increased the 5-year survival rates from 10 to 70% [3]. Magnetic resonance (MR) imaging plays a major role in preoperative assessment and planning for limb salvage surgery (LSS), as its precision has been shown from its early clinical advent for assessing tumor extent in bone marrow, and the surrounding soft tissues, as well as the relationship with the neurovascular bundles [4–10]. This modality is very sensitive in detecting a bone marrow edema pattern but has not been found to be specific enough to conclusively separate it from adjacent tumor [11]. False-positive interpretations result in more extensive unnecessary surgical resection, which may have a major impact on reconstruction, especially when involving the epiphysis side of a long bone. There are few studies in the literature that have attempted to define the role of MR imaging in delineating true tumor extent and in distinguishing it from peritumoral edema pattern, or peritumoral reaction, and correlating the findings with histology [4, 11–16].

Few of these studies focused on bone tumors extent only, with variable results.

This study aims to determine the role of MR imaging in interpreting abnormal signals within the bony compartment, in particular across the growth plate, and also in the soft tissues surrounding the tumor bulk, by correlating the MR findings with corresponding histopathological findings after wide surgical resection.

## Materials and methods

### Patients

This was a retrospective radiological-pathological review of all patients diagnosed and treated for primary bone sarcoma at the Children's Cancer Center of our institution between January 2002 and October 2010. This study was approved by the Institutional Review Board at our institution. Fifty-five patients were identified and 30 were enrolled in the study according to the following inclusion criteria: (1) diagnosis of osteosarcoma or Ewing's sarcoma, (2) readily available MR studies of the involved bone no more than 2 months prior to surgery, (3) presence of abnormal MR signal surrounding the tumor bulk within either bone or soft tissues, and (4) pathological material from the resected tumor with mapping grids. The 25 excluded patients did not meet one or more of the above inclusion criteria.

### Chemotherapy

All patients received neoadjuvant chemotherapy according to the current standard of care, except for one patient who had parosteal osteosarcoma. In brief, patients with non-metastatic osteosarcoma received therapy with a high dose of methotrexate, cisplatin, and doxorubicin. Patients with metastatic disease received additional cycles of a high dose of ifosfamide and etoposide. Patients with Ewing's sarcoma were treated with alternating cycles of vincristine, doxorubicin, cyclophosphamide, and ifosfamide/etoposide.

### MR examinations

All MR studies were obtained on a 1.5-Tesla MR unit (Intera NT; Philips; The Netherlands). All the analyzed MR examinations of the 30 enrolled patients were obtained after initiation of chemotherapy as follows: 11 patients had their MR imaging after completion of all cycles of neoadjuvant chemotherapy, while 19 patients had their MR imaging performed towards the end of treatment but before the last cycle of chemotherapy. The studies were performed in three planes (axial, coronal, and sagittal) depending on the location and extent of the tumor. Several sequences and

parameters were used, depending on the affected bone and the areas needed to be covered. These sequences included: (a) T1-weighted spin echo (TR=400–65, TE=10–18, slice thickness=5–8 mm, interval=0.6–0.8 mm, field of view (FOV)=210–500, NSA=2, matrix=256 × 256); (b) T2-weighted fast spin echo (TR=2,000–5,000, TE=100–130, slice thickness=5–8 mm, interval=0.5–0.8 mm, FOV=210–350, NSA=2, matrix=256 × 256); (c) short-tau inversion recovery (STIR) (TR=2,000–5,000, TE=70–100, TI=140–160, slice thickness=5–8 mm, interval=0.5–1.5, FOV=210–530, NSA=2, matrix=256 × 256); (d) T1-weighted fat-saturation (TR=400–600, TE=10–15, slice thickness=5–8 mm, interval=0.6–0.8, FOV=210–500, NSA=2, matrix=256 × 256) before and after intravenous gadolinium contrast administration (Dotarem 0.5 mmol/ml; Guerbet, France). All MR studies of the included patients were analyzed by a musculoskeletal radiologist (NJK) with 15 years of experience in musculoskeletal MR imaging. The radiologist was aware of the diagnosis of the primary lesion but was blinded to the patients' pathological results at resection. The radiologist focused his analysis on the MR sections that were in the same plane the tumor was bisected, on gross pathology, and which represented the largest surface area, as described later (e.g., Fig. 1a) (see below section on 'Pathological examination').

The areas of concern analyzed by MR imaging were those of non-mass-like abnormal signal intensity that were closely surrounding the tumor bulk, and at least partly inseparable from it. The demarcation between these areas and the tumor itself was established based on the identification of a definite, distinct, lobulated tumor, which frequently showed a low signal intensity corresponding to a pseudocapsule. The evaluated areas were reported in terms of location vis-à-vis the tumor bulk (e.g., medial, lateral, etc.), cranio-caudal (CC) extent, and thickness taken in a perpendicular plane to the CC extent (either transverse or anteroposterior (AP), depending on whether the analyzed section plane was coronal or sagittal). The areas of concern were also analyzed in terms of signal intensity (SI) relative to the tumor, and appearance (as elaborated in the Results section).

### Surgery

Wide resection was performed for all patients by the same surgical team (S.S. and R.H.). Twenty-six patients had prosthetic reconstruction, two had structural allografts, and two had no reconstruction (scapulectomy).

### Pathological examination and method of correlation with MRI

The gross specimens were examined according to a standard protocol. After orientation, the intact specimen was inked

and the soft tissue resection margins were sampled. Using an electric bandsaw, the specimen was then bisected along the plane that exposed the greatest tumor surface area. The cut surface was inspected and the extent of the lesion was measured. A 5-mm-thick slab of the entire cut surface was then obtained from the bisected specimen. The slab was fixed overnight in formalin, and later decalcified for a period of 24–48 h depending on the slab thickness as well as on the tumor and bone density. The slab was then photographed along with a metric ruler for subsequent construction of a grid map and measurements (e.g., Fig. 1b). Each section of the grid was submitted as one paraffin block. Hematoxylin

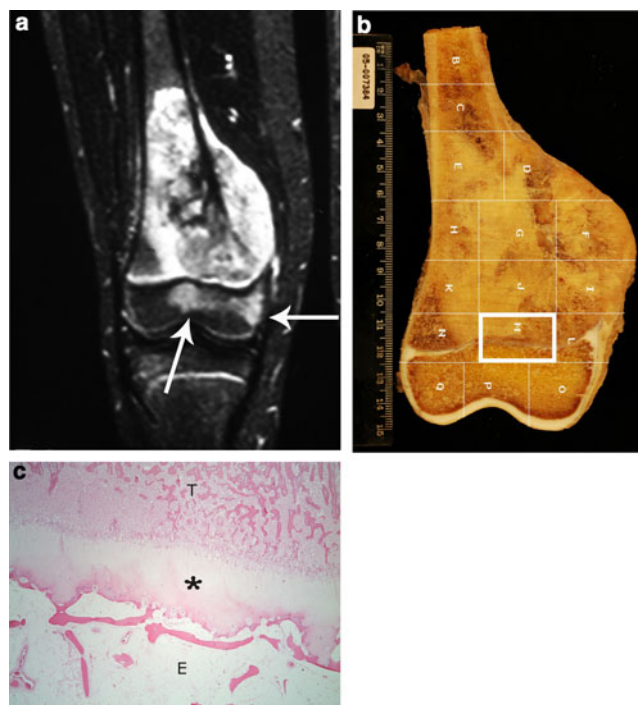


**Fig. 1** An 11-year-old male with right femoral osteoblastic osteosarcoma. **a** Coronal STIR (TR=2,500, TE=60) image of the right thigh showing a large heterogeneous tumor involving the distal femur reaching the growth plate and infiltrating the medial soft tissues. Focal areas of increased signal intensity are noted within the epiphysis, abutting the growth plate (*arrows*). These areas were of unclear histopathology. **b** Image of the coronal slab from the resected femur showing a large tumor reaching the growth plate. The mapping grid indicates the different block samples. The ruler helped in measuring the gross tumor size and extent as well as the exact location of the regions of interest detected on MRI. In this patient, the epiphyseal abnormal SI of concern corresponded to the distal medial grid sections (L, M, O, P). Analyses of all corresponding histopathology slides of these sections were done. The shape of the tissue section along with epiphyseal histological landmarks allowed the pathologist to identify and evaluate the area of concern within each section. **c** Histopathology from the grid section M (highlighted in the previous figure) (Hematoxylin and eosin [H&E], low magnification x20) revealing the osteoblastic osteosarcoma (T) abutting the growth plate (*asterisk*). The epiphysis (E) on the opposite end shows unremarkable bone trabeculae separated by marrow fat with no evidence of tumor cells or other abnormality. The three remaining grid sections (L, O, P) also showed normal epiphyseal tissue

and eosin (H&E)-stained sections corresponding to each block were obtained and given the same designation as that of the corresponding grid section.

In order to identify the grid section(s) to be analyzed for our study, an experienced bone pathologist (A.T.) and the radiologist (NJK) correlated the areas of concern seen on MRI with the gridded gross pathology slab, using the same orientation plane (i.e., coronal or sagittal) (e.g., Fig. 1a, b). The location and extent of these areas were determined by their distance from the articular surface in the specimen. The pathologist then examined all the H&E-stained slides of the selected grid section(s) to determine the nature of the areas of abnormal signal intensity (SI) seen on MR imaging. The shape of the tissue section along with histological landmarks (physis, cortex, gross tumor edge) allowed the pathologist to identify and evaluate the area of concern within each section (e.g., Fig. 1c). The findings were reported using five main categories: (1) normal (no pathological abnormalities), (2) edema, (3) fibrosis, (4) necrotic tumor, and (5) viable tumor. The examination included both soft tissue and bone marrow abnormalities that surrounded the tumor bulk on MR imaging.

#### Statistical analysis

Data are presented as median (range) or percentages. All bivariate comparisons were evaluated using the Mann–Whitney *U* test for continuous variables and the Fisher's exact and Spearman's test for categorical variables. All *p* values are two-tailed with the level of significance set at <0.05.

## Results

#### Patients and disease characteristics

Among the 30 patients who met our inclusion criteria, the male-to-female ratio was 16:14, with a median age of 12.5 years (range, 6–21 years). Twenty-seven patients had osteosarcoma and three patients had Ewing's sarcoma. Osteosarcoma was located in the following bones: femur (16 patients), tibia (eight patients), fibula (two patients), and humerus (one patient). Subtypes of osteosarcoma were: osteoblastic (21 patients), telangiectatic and chondroblastic (two patients from each), fibroblastic and parosteal (one patient in each). Ewing's sarcoma was found in the scapula (two patients) and femur (one patient).

#### MR imaging findings

Forty-six distinct areas of abnormal signal on MR imaging were investigated individually and correlated with the corresponding pathological examination, as per the methods

described previously. All these areas either surrounded or were at least partially inseparable from the tumor bulk. The CC extent of these areas ranged between 3 and 20 cm, while the thickness ranged between a few millimeters and 3 cm. In addition, several of the tumors had a hypointense rim, corresponding to a pseudocapsule, which also helped in differentiating the tumor bulk from its surroundings. This pseudocapsule was encountered in 17 tumors at the level of 22 analyzed areas.

As for the signal intensity, and in comparison to the tumor bulk, the analyzed areas were isointense on T1-weighted images showing diffuse enhancement following IV gadolinium administration similar to parts of the tumor bulk. On the T2-weighted and STIR sequences, 12 signals (26.1%) were higher in intensity than tumor, one (2.2%) was lower, and the remaining 33 (71.7%) were of similar intensity. When compared to intact muscles, all these areas showed increased SI on STIR and T2-weighted images.

The various areas of abnormal signal showed variable extension adjacent to the tumor, five being focal within the bone marrow. Within the soft tissues, the median CC extent of the signal abnormality was 7 cm (range, 3–20 cm).

When we further analyzed the MR characteristics and appearance of the abnormal peritumoral soft tissue (ST) signals, we could categorize them into three types: (1) the bulky type appearing as lobulated or thick localized tissue (>1 cm) confluent to the tumor bulk but distinct from it; (2) the feathery type, representing abnormal SI involving the muscles, whereby intact muscle bundles were seen within the abnormal high signal region, resulting in this feathery edema-like appearance; and (3) the linear fluid signal intensity area that was  $\leq 1$  cm in thickness.

#### MR imaging/pathology correlation

On pathological examination, 36 (78.3%) the analyzed areas were determined to be within the soft tissues surrounding and inseparable from the tumor bulk, while ten (21.7%) were seen in the nearby bone marrow, mostly at the level of the epiphysis (six areas). A total of 28 abnormal MR signals (21 in soft tissues, seven in bones) were histologically free of tumor and of any abnormalities, and were considered histologically normal (category 1; 60.9%) (Figs. 1, 2, 3). The remaining 18 (39.1%) corresponded to one of the four following categories: four (three in soft tissues, one in bone) were found to have edema (category 2; 8.7%) (Fig. 3), six (all in soft tissues) revealed fibrosis (category 3; 13.05%) (Fig. 4), two (one in soft tissues, one in bone) had necrotic tumor (category 4; 4.3%) (Fig. 5), six (five in soft tissues, one in bone) were found to have viable tumor (category 5; 13.05%) (Fig. 6). In the soft tissues, these pathologic findings corresponded to the various MR



characteristics described above. The MR/pathology correlation within the soft tissues is summarized in Table 1.

There was no statistically significant correlation between patients' age, gender, extent of the abnormal areas around the tumor, its SI relative to the tumor, or analyzed tissue area (i.e., bone marrow or soft tissue) and the tumor involvement (viable or necrotic tumor) on pathological examination. However, there was a statistically significant correlation between presence or absence of tumor cells and the MR characteristics of the surrounding abnormal soft tissue. In fact, a feathery edema-like appearance seen in 18 investigated areas corresponded in all cases to tumor-negative areas (Figs. 2 and 4); whereas a bulky or thick appearance correlated with the presence of tumor cells, either necrotic or viable, in five out of seven areas (Figs. 5 and 6) (Table 2).

In the 22 analyzed areas where the primary tumors had a pseudocapsule (Figs. 2, 4, and 6), 18 areas (82%) showed no evidence of tumor cells and four areas (18%) showed viable tumor cells. Among all eight cases where tumor cells were present, four had pseudocapsule.

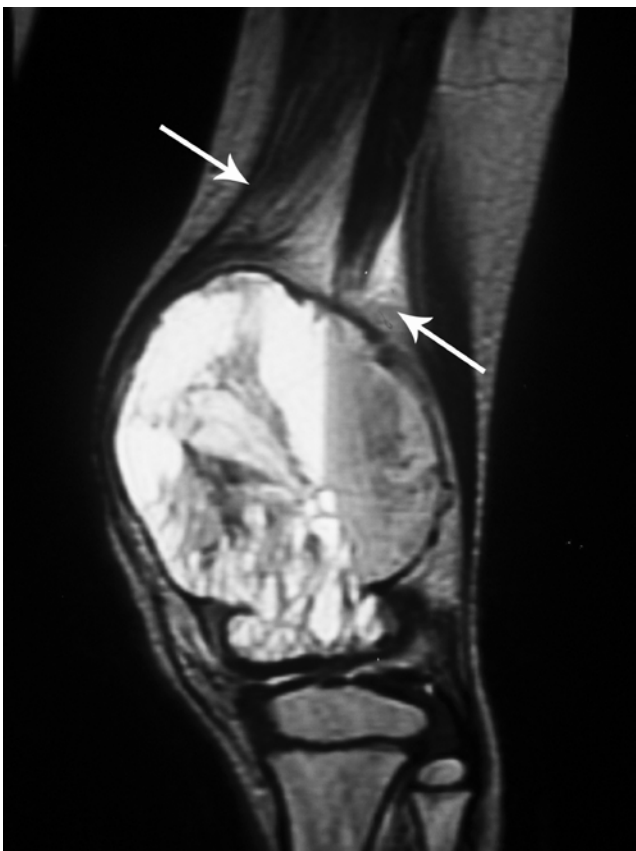


**Fig. 2** An 8-year-old male with osteoblastic/telangiectatic osteosarcoma of the distal right femur. Sagittal T2-weighted (TR=2,500, TE=100) image showing a large heterogeneous mass with fluid–fluid levels. The tumor has low signal intensity rim (pseudocapsule). Superiorly, there is a feathery high SI edema-like appearance of the soft tissues (arrows), proven to be normal on corresponding histopathology sections

## Discussion

Our study has demonstrated that abnormal signals surrounding or adjacent to the tumor bulk on MR imaging of osteosarcoma and Ewing's sarcoma after chemotherapy are most often not associated with tumor involvement at pathological evaluation. We documented that 17.4% of these signals correspond to tumor involvement, and that 13.3% of the

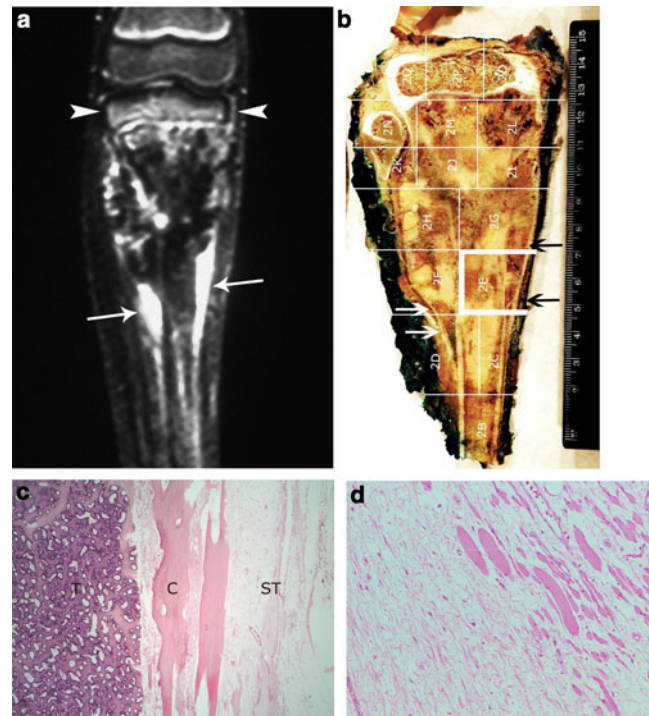


**Fig. 3** An 11-year-old male with right tibial osteoblastic osteosarcoma. **a** Coronal STIR (TR=2,500, TE=60) image of the right leg. The tumor is of low signal intensity, involving the proximal meta-diaphyses and reaching the physis. Inferiorly, both medially and laterally, linear areas of increased signal were identified within the deep soft tissues (arrows) adjacent to the involved tibia, each measuring  $\leq 1$  cm in thickness. Patchy increased signal was noted in the proximal epiphysis (arrowheads). **b** Image of the coronal slab from the resected portions of the tibia and fibula shows the large tibial tumor reaching the proximal growth plate. The mapping grid indicates the different block samples. The distance of the concerned areas seen on MRI from the tibial plateau and their cranio-caudal extent allowed their identification on the gross specimen (white and black arrows) by using the adjacent ruler. These areas corresponded to the medial grid sections (2E, 2G; black arrows) and to the lateral grid sections (2D, 2F; white arrows). The shape of the tissue section along with the intramedullary mass as histological landmark allowed the pathologist to identify and evaluate the area of concern within these sections. **c** Histopathology of the grid section 2E (highlighted in the previous figure) (H&E, low magnification x20) showing cortical bone (C) separating residual intramedullary malignant osteoid (T) from surrounding swollen and edematous soft tissues (ST). **d** High magnification representative photomicrograph taken from the most lateral portion of the same 2E section (H&E, original magnification x200) demonstrates edema appreciated as clearing that is causing separation of collagen fibers and some skeletal muscle fibers. The tibial epiphysis showed normal histopathology on the slides taken from the corresponding sections (2O, 2P, 2Q)

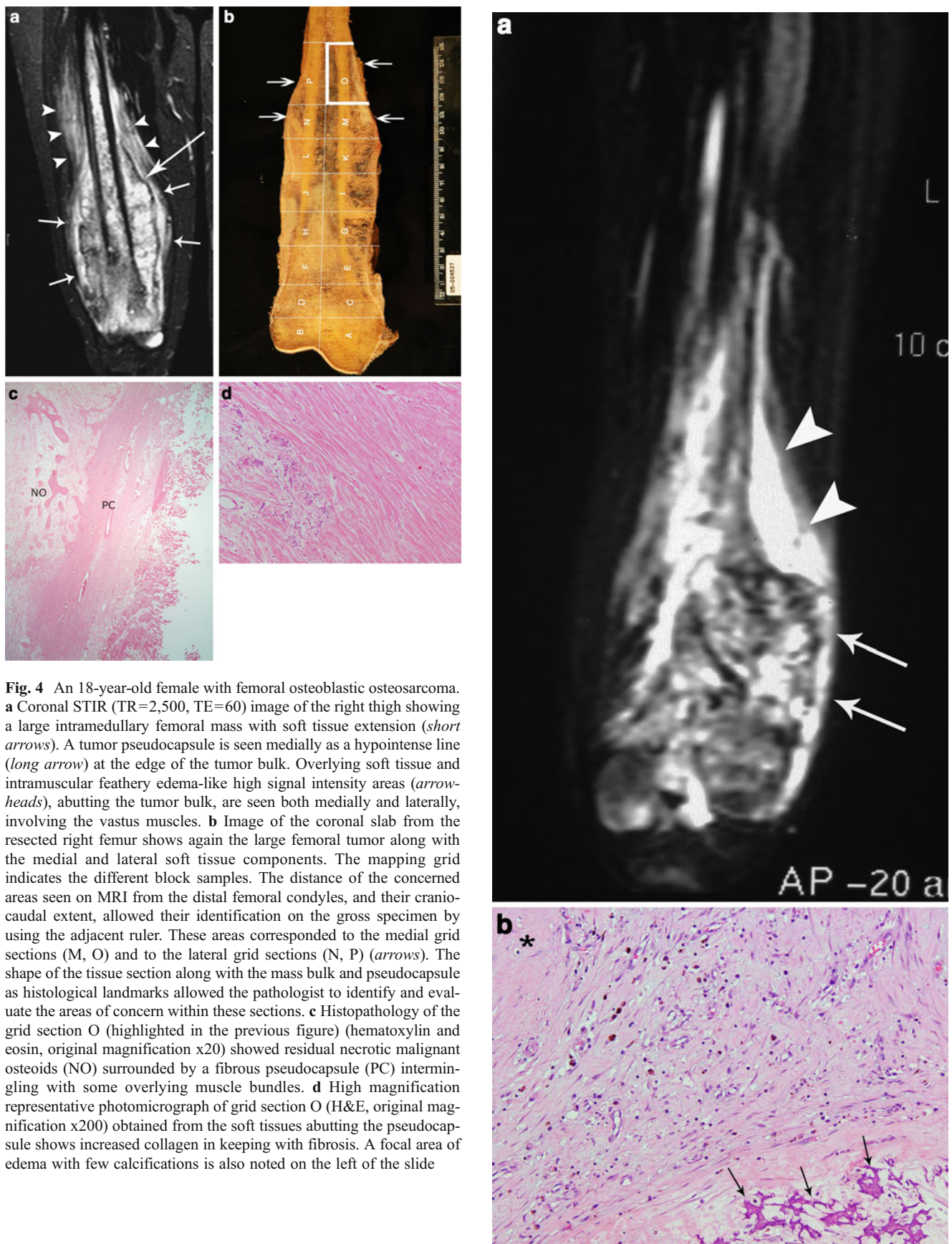


**Fig. 4** An 18-year-old female with femoral osteoblastic osteosarcoma. **a** Coronal STIR (TR=2,500, TE=60) image of the right thigh showing a large intramedullary mass with soft tissue extension (*short arrows*). A tumor pseudocapsule is seen medially as a hypointense line (*long arrow*) at the edge of the tumor bulk. Overlying soft tissue and intramuscular feathery edema-like high signal intensity areas (*arrowheads*), abutting the tumor bulk, are seen both medially and laterally, involving the vastus muscles. **b** Image of the coronal slab from the resected right femur shows again the large femoral tumor along with the medial and lateral soft tissue components. The mapping grid indicates the different block samples. The distance of the concerned areas seen on MRI from the distal femoral condyles, and their craniocaudal extent, allowed their identification on the gross specimen by using the adjacent ruler. These areas corresponded to the medial grid sections (M, O) and to the lateral grid sections (N, P) (*arrows*). The shape of the tissue section along with the mass bulk and pseudocapsule as histological landmarks allowed the pathologist to identify and evaluate the areas of concern within these sections. **c** Histopathology of the grid section O (highlighted in the previous figure) (hematoxylin and eosin, original magnification x20) showed residual necrotic malignant osteoids (NO) surrounded by a fibrous pseudocapsule (PC) intermingling with some overlying muscle bundles. **d** High magnification representative photomicrograph of grid section O (H&E, original magnification x200) obtained from the soft tissues abutting the pseudocapsule shows increased collagen in keeping with fibrosis. A focal area of edema with few calcifications is also noted on the left of the slide



**Fig. 5** A 12-year-old female with femoral osteoblastic osteosarcoma. **a** Coronal STIR (TR=4,652, TE=70) image of the thigh showing a distal heterogeneous left femoral tumor with a large soft tissue component (*arrows*). Supero-laterally, there is a triangular bulky area of high signal intensity (*arrowheads*) involving the vastus lateralis muscle that appears adjacent to the tumor bulk and distinct from it. This area is iso-intense to the areas of high signal within the tumor. **b** Photomicrograph of the triangular area of concern demonstrating mostly granulation tissue in an area of necrotic tumor. Shadows of necrotic tumor cells can be seen (*asterisk*). Calcifications are also noted (*arrows*) (H&E, original magnification x400)

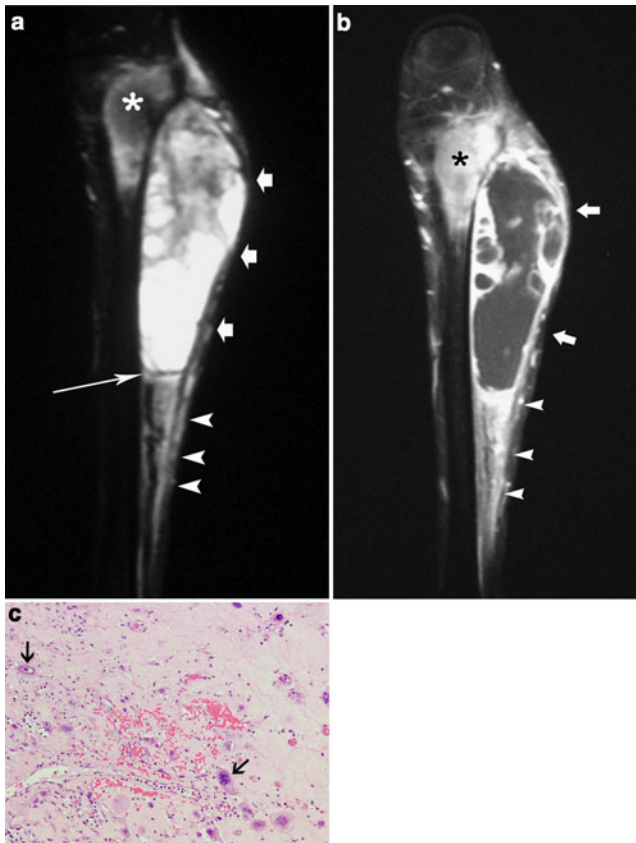


**Fig. 6** A 17-year-old female with right tibial osteoblastic osteosarcoma. **a** Coronal STIR (TR=2,500, TE=60) image showing a heterogeneous proximal tibial tumor (*asterisk*) with large soft tissue component (*short arrows*). Inferior to the soft tissue tumor component, there is a thick intermediate signal intensity area (*arrowheads*) separate from the tumor bulk by a low intensity pseudocapsule (*long arrow*). **b** Coronal T1-weighted fat-saturation after IV gadolinium administration (TR=500, TE=18) image showing enhancement of the intramedullary tumor component (*asterisk*). A significant proportion of the soft tissue component of the tumor (*short arrows*) does not enhance, in keeping with necrosis. The area of concern (*arrowheads*), inferior to the tumor soft tissue component, shows enhancement similar to some portions of the tumor. **c** Histopathology of the abnormal area inferior to the tumor bulk shows scattered residual viable tumor cells (*arrows*). These cells have markedly enlarged pleomorphic and hyperchromatic nuclei with prominent nucleoli. (H&E, original magnification x400)

**Table 1** Histopathological categories corresponding to the various MR appearances seen in 36 soft tissue areas surrounding bone sarcomas

MR appearance	Histological categories				
	Normal <i>n</i> =21	Edema <i>n</i> =3	Fibrosis <i>n</i> =6	Necrotic <i>n</i> =1	Viable <i>n</i> =5
Bulky or thick <sup>a</sup>	1	0	1	1	4
Feathery	13	2	3	0	0
Linear <sup>b</sup>	7	1	2	0	1

<sup>a</sup>>1 cm in thickness

<sup>b</sup>≤1 cm in thickness

analyzed areas represent viable tumor. In addition, when detailed description of the soft tissue components surrounding the tumor was analyzed, we could demonstrate that the feathery edema-like pattern of signal intensity (Figs. 2 and 4) correlated with non-tumoral tissue (normal tissue, fibrosis, or edema), whereas a bulky or thick appearance confluent to the mass (Figs. 5 and 6) corresponds to areas of tumor involvement. These findings may influence the orthopedic surgeon's decision when faced with the possibility of amputation versus extent of limb salvage procedure, particularly important when the area in question is around the physis. In our population, we found that 82.6% of abnormal areas surrounding the tumor bulk appeared free of tumor. This is in contradistinction to previous studies dealing with soft tissue sarcomas whereby abnormal areas beyond the tumor bulk (reactive zone) frequently contained tumor cells [17]. In addition, none of our patients with a feathery edema-like soft tissue appearance on MR had histological evidence of positive tumor. The number of abnormal areas within the bone marrow was too small to convey statistical significance. We, however, found that in the four cases with grossly intact physis, the epiphyseal abnormal signal was

**Table 2** Statistical analysis correlating the appearance of MR signals abnormality within the soft tissues and tumor-positive or tumor-negative pathology specimens

Soft tissue appearance	Tumor-negative (categories 1, 2, 3) <i>n</i> =30	Tumor-positive (categories 4, 5) <i>n</i> =6	<i>p</i> value
Bulky or thick <sup>a</sup> , <i>n</i> (%)	2 (6.7)	5 (83.3)	< 0.001
Feathery, <i>n</i> (%)	18 (60)	0 (0)	0.019
Linear <sup>b</sup> , <i>n</i> (%)	10 (33.3)	1 (16.7)	0.643

<sup>a</sup>>1 cm in thickness

<sup>b</sup>≤1 cm in thickness

not involved with tumor (Fig. 1). Presence of tumor pseudocapsule was not helpful in defining the nature of tumor infiltration in surrounding tissues.

The prognosis of patients with bone sarcomas has improved significantly over the past three decades, with MR imaging playing a major role in determining the initial diagnosis, prognosis, and pre-operative planning [7, 8, 10, 11, 18]. Additionally, sarcomas are being treated definitively with LSS rather than amputations. MR imaging has been instrumental in planning these procedures. It is useful in evaluating the intraosseous extent, bone marrow and neurovascular involvement, skip metastases, and epiphyseal extension of tumor in the extremities [4–6, 9, 11]. By identifying the extent of the tumor, adequate resection is achieved, while normal uninvolved tissue is preserved, reducing post-operative morbidity and improving limb function [19].

Several studies have addressed the issue of whether true tumor extent can be defined by MR imaging in the presence of abnormal signal changes adjacent or confluent with the easily recognized tumor bulk [4, 12–16]. Some of these studies covered a heterogeneous group of both soft tissue and bone tumors [15, 16]. Sanchez et al. found that areas of high SI on T2-weighted images may correspond to viable tumor, tumor necrosis, edema, fibrosis, or hemorrhage, yet there were no distinguishing features by MRI [13]. Others found that both tumor and peritumoral edema had high SI on T2-weighted or STIR images but could not be differentiated [14, 16]. Our data reveal similar findings in that the abnormal areas were all of high SI on T2-weighted and STIR images and corresponded to the five different pathological categories, described in the ‘Results’ section, but the SI was not helpful in assessing the pathological nature of these areas. Previous studies have evaluated the value of IV gadolinium administration in assessing true tumor extent. In one study, this was not found to be helpful [4], as was the case in our series where all areas of concern showed some enhancement regardless of their histological nature. Other reports showed that dynamic post-contrast images allowed differentiation between viable tumor and non-neoplastic edema or necrotic tumor [12, 14, 20]. We do not routinely employ dynamic contrast examinations.

The authors understand the limitations inherent to all retrospective studies; however, blinding was maintained to the pathological diagnosis of the studied areas. Additionally, the number of patients, as is often the case when dealing with sarcomas, and the number of analyzed areas including those with tumor cells were too small for adequate statistical analysis. Finally, the MR images used were those closest to the index surgery, yet some patients underwent their final cycle of chemotherapy following their last MR examination. However, those who underwent chemotherapy following MR imaging only experienced one dose and not the whole

cycle of neoadjuvant chemotherapy. Besides, we considered areas with viable tumor or tumor necrosis as positive in our analysis and all other findings as negative. Thus, we are unlikely to have falsely underestimated tumors.

In summary, we found that tumor involvement in areas of abnormal MR signal surrounding osteosarcoma and Ewing’s sarcoma post chemotherapy in children and not associated with bulk is uncommon. MR imaging is helpful in predicting the nature of these areas, which are usually tumor-free on pathology when the signal in the soft tissues around the tumor is feathery and not bulky. This will help the orthopedic surgeon preserve enough soft tissue for limb salvage and/or increased function if the reactive zone, as these non-tumorous areas represent, is preserved. However, we found that the extent and intensity of these signals were generally unhelpful in delineating tumor involvement. Larger studies are called for to confirm our findings and prospectively evaluate their effect on decision-making in the surgical treatment of bone sarcomas.

**Acknowledgements** The authors would like to thank The Board of Trustees of the Children’s Cancer Center of Lebanon Foundation and the International Outreach Program at the St. Jude Children’s Research Hospital, Memphis, TN, USA, for their continuous support. The authors would also like to thank Dr. Monique Chaaya (Chair, Department of Epidemiology & Population Health, American University of Beirut, Beirut, Lebanon) for her assistance in statistical analysis.

## References

1. Herzog CE. Overview of sarcomas in the adolescent and young adult population. *J Pediatr Hematol Oncol.* 2005;27(4):215–8.
2. Caudill JS, Arndt CA. Diagnosis and management of bone malignancy in adolescence. *Adolesc Med State Art Rev.* 2007;18(1):62–78. ix.
3. Longhi A, Errani C, De Paolis M, et al. Primary bone osteosarcoma in the pediatric age: state of the art. *Cancer Treat Rev.* 2006;32:423–36.
4. Seeger LL, Widoff BE, Bassett LW, et al. Preoperative evaluation of osteosarcoma: Value of gadopentate dimeglumine-enhanced MR imaging. *AJR.* 1991;157:347–51.
5. Onikul E, Fletcher BD, Parham DM, et al. Accuracy of MR imaging for estimating intraosseous extent of osteosarcoma. *AJR.* 1996;167:1211–5.
6. Sundaram M, McGuire MH, Herbold DR, Wolverson MK, Heiberg E, et al. Magnetic resonance imaging in planning limb-salvage surgery for primary malignant tumors of bone. *J Bone Joint Surg Am.* 1986;68:809–19.
7. Brisse H, Ollivier L, Edeline V, et al. Imaging of malignant tumours of the long bones in children: monitoring response to neoadjuvant chemotherapy and preoperative assessment. *Pediatr Radiol.* 2004;34:595–605.
8. Kaste SC. Imaging pediatric bone sarcomas. *Radiol Clin North Am.* 2011;49(4):749–65. vi-vii.
9. Panuel M, Gentet JC, Scheiner C, et al. Physeal and epiphyseal extent of primary malignant bone tumors in childhood. Correlation of preoperative MRI and the pathologic examination. *Pediatr Radiol.* 1993;23(6):421–4.



10. Schima W, Amann G, Stiglbauer R, et al. Preoperative staging of osteosarcoma: efficacy of MR imaging in detecting joint involvement. *Am J Roentgenol*. 1994;163(5):1171–5.
11. Hoffer FA, Nikanorov AY, Reddick WE, et al. Accuracy of MR imaging for detecting epiphyseal extension of osteosarcoma. *Pediatr Radiol*. 2000;30:289–98.
12. Erlemann R, Reiser MF, Peters PE, et al. Musculoskeletal neoplasms: static and dynamic Gd-DTPA-enhanced MR imaging. *Radiology*. 1989;171(3):767–73.
13. Sanchez RB, Quinn SF, Walling A, et al. Musculoskeletal neoplasms after intraarterial chemotherapy: correlation of MR images with pathologic specimens. *Radiology*. 1990;174(1):237–40.
14. Lang P, Honda G, Roberts T, et al. Musculoskeletal neoplasm: perineoplastic edema versus tumor on dynamic postcontrast MR images with spatial mapping of instantaneous enhancement rates. *Radiology*. 1995;197(3):831–9. Erratum in: *Radiology* 1996;198(3):910–911.
15. Beltran J, Simon DC, Katz W, et al. Increased MR signal intensity in skeletal muscle adjacent to malignant tumors: pathologic correlation and clinical relevance. *Radiology*. 1987;162(1 Pt 1):251–5.
16. Shuman WP, Patten RM, Baron RL, et al. Comparison of STIR and spin-echo MR imaging at 1.5 T in 45 suspected extremity tumors: lesion conspicuity and extent. *Radiology*. 1991;179(1):247–52.
17. White LM, Wunder JS, Bell RS, et al. Histologic assessment of peritumoral edema in soft tissue sarcoma. *Int J Radiat Oncol Biol Phys*. 2005;61(5):1439–45.
18. Lawrence JA, Babyn PS, Chan HS, et al. Extremity osteosarcoma in childhood: prognostic value of radiologic imaging. *Radiology*. 1993;189:43–7.
19. McDonald DJ. Limb-salvage surgery for treatment of sarcomas of the extremities. *AJR*. 1994;163(3):509–13.
20. James SL, Panicek DM, Davies AM. Bone marrow oedema associated with benign and malignant bone tumours. *Eur J Radiol*. 2008;67(1):11–21.